Sliding Mode Control of a Shape Memory Alloy Actuated Manipulator

Mohammad H. Elahinia*, T. Michael Siegler, Donald J. Leo , and Mehdi Ahmadian

Department of Mechanical Engineering
Virginia Polytechnic and State University
Blacksburg, VA 24061

email: elahinia@vt.edu

ABSTRACT

This paper presents a two-part controller that uses a state variable estimator for control of a single degree of freedom rotary manipulator actuated by Shape Memory Alloy (SMA) wire. A model for the SMA actuated manipulator is presented. The model includes nonlinear dynamics of the manipulator, a constitutive model of the Shape Memory Alloy, and the electrical and heat transfer behavior of SMA wire. The estimator predicts the state vector at each time step and corrects its prediction based on the angular position measurements. The transformation temperatures of the SMA wire are stress dependent: this adds to complexity of the control of the position of the arm for certain angular positions. To overcome this problem a sliding mode controller is designed to calculate the desired stress of the wire based on the desired angular position of the arm. A classical feedback controller maintains this desired stress by regulating the input voltage to the SMA wire. The stress of the wire is a better set-point for the controller since the transformation temperatures and hence the Martensite fraction are functions of the wire's stress. The stabilization and tracking performance of this two-part controller is presented and compared with a PID controller.

I. INTRODUCTION

SMAs consist of a group of metallic materials that demonstrate the ability to return to some previously defined shape or size when subjected to the appropriate thermal procedure. The shape memory effect is hysteretic and occurs due to a temperature and stress dependent shift in the materials crystalline structure between two different phases called Martensite and Austenite which are the low and high temperature phases, respectively. SMA actuators have several advantages for miniaturization such as excellent power to mass ratio, maintainability, reliability, and clean and silent actuation. The disadvantages are low energy efficiency due to conversion of heat to mechanical energy and inaccurate motion control due to hysteresis, nonlinearities, parameter uncertainties, and difficulty in measuring variables such as temperature.

The control research applied to SMAs may be divided into three categories of linear control, Pulse Width Modulation (PWM), and nonlinear control. Different variations of linear Proportional Integral Derivative (PID) controls have been explored by several researchers [1]–[6] while many others have used PWM [7]–[10]. Several nonlinear control schemes such as fuzzy logic, feedback linearization, sliding mode, adaptive, and variable structure control have also been explored by researchers [11]–[23].

In this work, for controlling the angular position of an SMA-actuated manipulator, we have developed a sliding mode controller that works in conjunction with a classical feedback controller. The feedforward sliding mode controller computes the desired stress of the SMA wire according to the desired angular position of the arm and the feedback controller adjusts the control input (voltage) to maintain the desired stress in the wire. The controller uses an Extended Kalman Filter (EKF) to estimate the stress of the SMA wire. The arm is actuated by a bias type actuator constructed with SMA wire, pulleys, and a linear spring. A nonlinear model is developed based on the arm nonlinear dynamic model, an SMA wire constitutive model, an SMA phase transformation model [24], [25], and a nonlinear heat convection model [14], [26]. This model has been experimentally verified by Elahinia and Ashrafiuon [14]. The Extended Kalman Filter has been designed for an SMA actuated manipulator and was tested through simulations in our other works [27], [28]. The EKF utilizes the control input and the angular position of the arm to predict the other state variables of the system: angular velocity, SMA wire stress, and SMA wire temperature. Since the sliding mode controller transforms the nonlinear dynamics of the arm into a first order system the resulting control algorithm has a better overall performance both in stabilization and tracking in the presence of model uncertainties.

II. THE SMA ARM MODEL

The single degree-of-freedom (1-dof) SMA-actuated arm is shown in Fig. 1. We have used $150\mu m$ diameter Ni-Ti SMA wire which is actuated by electrical heating [14]. The net actuating torque is the difference between the resulting bias spring and SMA wire torques. The SMA arm model consists of phase transformation, heat transfer, SMA wire constitutive, and arm dynamic blocks.

A. Kinematic/Dynamic model

The nonlinear dynamic model of the arm including spring and payload effects is represented by:

$$I_e\ddot{\theta} = \tau_{\mathrm{w}}(\sigma) - \tau_{\mathrm{g}}(\theta) - \tau_{\mathrm{s}}(\theta) - c\dot{\theta} \qquad (1)$$

Report Documentation Page

Form Approved
OMB No. 0704-0188

1. REPORT DATE	2. REPORT TYPE	3. DATES COVERED
00 JUN 2003	**N/A**	**-**

4. TITLE AND SUBTITLE	5a. CONTRACT NUMBER
Sliding Mode Control of a Shape Memory Alloy Actuated Manipulator	5b. GRANT NUMBER
	5c. PROGRAM ELEMENT NUMBER
6. AUTHOR(S)	5d. PROJECT NUMBER
	5e. TASK NUMBER
	5f. WORK UNIT NUMBER
7. PERFORMING ORGANIZATION NAME(S) AND ADDRESS(ES) **Department of Mechanical Engineering Virginia Polytechnic and State University Blacksburg, VA 24061**	8. PERFORMING ORGANIZATION REPORT NUMBER
9. SPONSORING/MONITORING AGENCY NAME(S) AND ADDRESS(ES)	10. SPONSOR/MONITOR'S ACRONYM(S)
	11. SPONSOR/MONITOR'S REPORT NUMBER(S)

12. DISTRIBUTION/AVAILABILITY STATEMENT
Approved for public release, distribution unlimited

13. SUPPLEMENTARY NOTES
See also ADM001697, ARO-44924.1-EG-CF, International Conference on Intelligent Materials (5th) (Smart Systems & Nanotechnology)., The original document contains color images.

14. ABSTRACT

15. SUBJECT TERMS

16. SECURITY CLASSIFICATION OF:			17. LIMITATION OF ABSTRACT	18. NUMBER OF PAGES	19a. NAME OF RESPONSIBLE PERSON
a. REPORT	b. ABSTRACT	c. THIS PAGE			
unclassified	**unclassified**	**unclassified**	**UU**	**7**	

where θ is the angular position of the arm, $\tau_{\rm w}, \tau_{\rm g}$, and $\tau_{\rm s}$ are the resulting torques from SMA wire, gravitational loads, and the bias spring, respectively, and σ is the wire stress. I_e is the effective mass moment of inertia of the arm, gripper, and the payload, and c is the torsional damping coefficient approximating the net joint friction.

The SMA wire strain rate $\dot{\varepsilon}$ and joint angular velocity $\dot{\theta}$ are related kinematically as:

$$\dot{\varepsilon} = -\frac{2r_{\rm p}\dot{\theta}}{l_0} \tag{2}$$

where $r_{\rm p}$ is pulleys radius and l_0 is the initial length of the SMA wire.

B. Wire constitutive model

The wire constitutive model shows the relationship between stress rate ($\dot{\sigma}$), strain rate, and temperature rate ($\dot{T}$) [29]:

$$\dot{\sigma} = D\dot{\varepsilon} + \theta_T\dot{T} + \Omega\dot{\xi} \tag{3}$$

where $D = \frac{D_M + D_A}{2}$ is (the average) Young modulus, D_A is Austenite Young modulus, D_M is Martensite Young modulus, θ_T is thermal expansion factor, $\Omega = -D\varepsilon_0$ is phase transformation contribution factor, and ε_0 is the initial (i.e. maximum) strain [24].

C. SMA Wire Phase Transformation Model

Due to hysteretic behavior of SMA wire, the phase transformation equations are different for different load and heating conditions. The reverse transformation from Martensite to Austenite takes place as a result of heating or unloading

$$\dot{\xi} = -\frac{\xi_M}{2}\sin[a_A(T - A_s - \frac{\sigma}{C_A})][a_A\dot{T} - \frac{a_A}{C_A}\dot{\sigma}] \tag{4}$$

if $C_A(T - A_f) < \sigma < C_A(T - A_s)$. Where $0 \leq \xi \leq 1$ is the Martensite fraction coefficient, ξ_M is the maximum Martensite fraction obtained during cooling, T is the SMA wire temperature, A_s and A_f are Austenite phase start and final temperatures, and $a_A = \frac{\pi}{A_f - A_s}$, $b_A = \frac{-a_A}{C_A}$ and C_A are curve fitting parameters. The forward transformation equation from Austenite to Martensite takes place because of cooling or loading

$$\dot{\xi} = -\frac{1 - \xi_A}{2}\sin[a_M(T - M_f - \frac{\sigma}{C_M})][a_M\dot{T} - \frac{a_M}{C_M}\dot{\sigma}] \tag{5}$$

if $C_M(T - M_s) < \sigma < C_M(T - M_f)$. Where ξ_A is the minimum Martensite fraction obtained during heating, M_s and M_f are Martensite phase start and final temperatures, and $a_M = \frac{\pi}{M_s - M_f}$, $b_M = \frac{-a_M}{C_M}$ and C_M are curve fitting parameters.

D. Heat transfer model

The SMA wire heat transfer equation consists of electrical heating and natural convection:

$$mc_p\frac{dT}{dt} = \frac{V^2}{R} - hA_c(T - T_\infty) \tag{6}$$

where R is resistance per unit length, c_p is the specific heat, m is mass per unit length and A_c is circumferential area of the SMA wire. Also, V is the applied voltage, T_∞ is the ambient temperature, and h is heat convection coefficient.

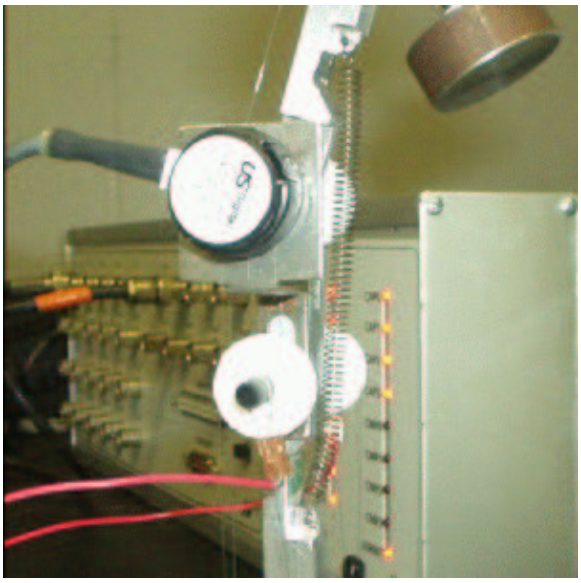

Fig. 1. The 1-dof SMA arm, actuated by NiTi wire and a bias spring

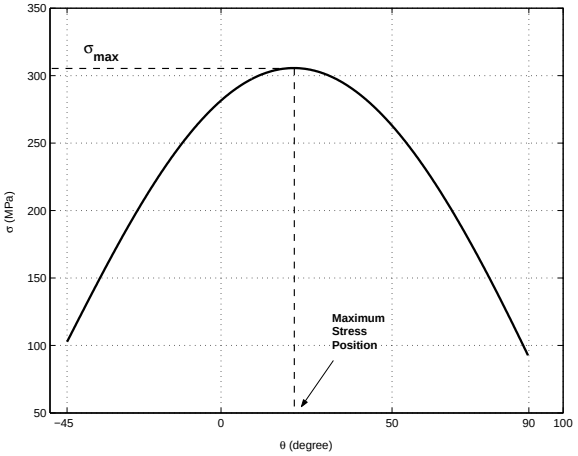

Fig. 2. The static stress of the wire as a function of the angular position of the arm

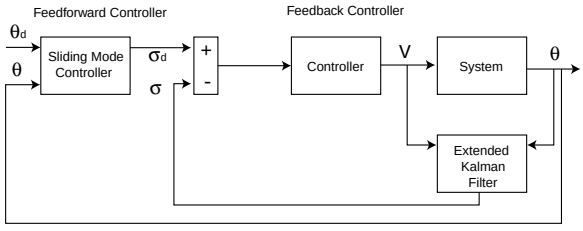

Fig. 3. The feedforward-feedback controller schematic and the Extended Kalman Filter

III. CONTROL

The SMA phase transformation temperatures are affected by the stress of the wire. Therefore when the arm moves beyond a certain angular position, at which the stress of the wire is maximum, the transformation temperatures decrease. Figure 2 shows the static stress of the wire as a function of the angular position of the arm. If the desired angular position is beyond this maximum stress position, the control system should first apply high enough voltage in order for the wire to go through phase transformation and therefore reach the maximum stress. Beyond this position, while the position error is still not zero, the voltage should drop rapidly in order to prevent the wire's temperature from going beyond A_f which causes the full phase transformation. Therefore, if a control system works based on the position error only, even when the arm is beyond the maximum stress position it will apply high voltage to the wire; hence the wire will be overheated and the arm will exceed the desired angular position. Although it is possible to tune such a position-based controller to work well for certain positions it cannot work well for all the set-points.

One way to solve this problem is to design a controller that works based on the stress of the SMA wire. In this section a sliding mode controller is designed to calculate the desired stress of the wire based on the desired angular position. A second feedback controller, which is a PID controller, is used to maintain this desired stress by applying the required voltage to the SMA wire. Since this two-part controller tracks the desired stress of the wire, when the arm reaches the maximum stress position, the controller adjust the control input accordingly. Therefore the wire will not overheat. The control system is shown schematically in Fig. 3. The actual stress of the wire is estimated using an Extended Kalman Filter, which was designed in our previous work [27].

Sliding control is a robust nonlinear Lyapunov-based control algorithm in which an nth order nonlinear and uncertain system is transformed to a 1st order system. Let's consider the SISO system

$$x^{(n)} = f(\mathbf{x}) + b(\mathbf{x})u \tag{7}$$

where u and x are the scalar input and output respectively and $\mathbf{x}$ is the state vector. For this system the nonlinear functions f and b are not exactly known. The control objective is for the system to follow a desired state vector $\mathbf{x}_d$. Furthermore consider the time-varying surface $S(t)$ in the state-space

$$s(\mathbf{x}, t) = (\frac{d}{dt} + \lambda)^{n-1}\widetilde{x} \tag{8}$$

where $\widetilde{x} = x - x_d$ is the tracking error and λ is a positive constant. It can be shown that tracking the desired state vector is equivalent to remaining on the surface $S(t)$ [30]. Therefore the control law should be selected in a way that the distance to this surface decreases along all system trajectories

$$\frac{1}{2}\frac{d}{dt}s^2 \leq \eta s \tag{9}$$

where η is a positive constant; equation 9 is called the sliding condition. As the result all the trajectories are forced to reach the sliding surface in finite time and stay on the surface for all future times. $S(t)$ is called the sliding surface and the systems behavior once on the surface is called sliding mode ($\dot{s} = 0$). It can be shown that the reach time from the initial state to the surface is [30]

$$t_{\text{reach}} \leq s(t = 0)/\eta \tag{10}$$

Thus a typical motion under sliding mode control consists of reaching phase and sliding phase during which the motion is confined to the sliding surface. Further details on the sliding mode control can be found in [30], [31].

A. Controller design

The sliding controller in this work is deigned to calculate the desired stress of the SMA wire. Considering the equation of motion (equation 1), the sliding surface can be defined as

$$s = (\frac{d}{dt} + \lambda)\widetilde{\theta} \tag{11}$$

where $\widetilde{\theta} = \theta - \theta_d$. The dynamic of the system once on the sliding surface can be written as

$$\dot{s} = 0 \tag{12}$$

This equation describes the dynamic of the system while in the sliding mode and can be used to find the desired torque of the wire:

$$\begin{aligned} \dot{s} &= \ddot{\theta} - \ddot{\theta}_d + \lambda\dot{\widetilde{\theta}} = (\tau_{\text{w}} - \tau_{\text{g}} - \tau_{\text{s}} - c\dot{\theta})/I_e \\ &- \ddot{\theta}_d + \lambda\dot{\widetilde{\theta}} = 0 \end{aligned} \tag{13}$$

and therefore

$$\begin{aligned} \tau_{\text{w}} &= \tau_{\text{g}} + \tau_{\text{s}} + c\dot{\theta} + I_e\ddot{\theta}_d - I_e\lambda\dot{\widetilde{\theta}} \\ &+ K\text{sat}(s) \end{aligned} \tag{14}$$

where K is the control gain. The saturation term is added to the desired torque in order to address the uncertainties in the model. This term also causes the trajectories to merge to the sliding surface when the initial state of the system is not on the sliding surface ($\widetilde{\theta}(0) \neq 0$). The desired stress of the SMA wire can be readily calculated using the desired torque of equation 13 .

IV. RESULTS

The nonlinear SMA model used for the simulations in this work has been previously verified through several experiments [14]. Figure 4 shows the simulation and experimental results for two different voltages. Using this model, in this section, the simulation results with the sliding mode controller (SLD) is presented and compared with a PID controller. Figure 5 compares the regulation performance of the proposed controller with that of a PID controller. The PID controller, which works based on the position error, can be tuned to perform well for certain set-points while the same SLD controller works well for all the desired positions. The regulation performance of the SLD controller for several set-points is shown in Fig. 6. It can be seen that the arm reaches the desired position for all the set-points in less than 4 sec even though small overshoots exist. The performance of the controller in tracking the desired

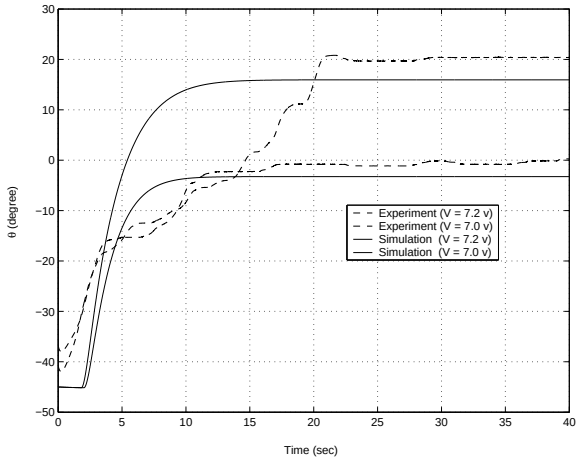

Fig. 4. Comparing open-loop simulation and experimental results

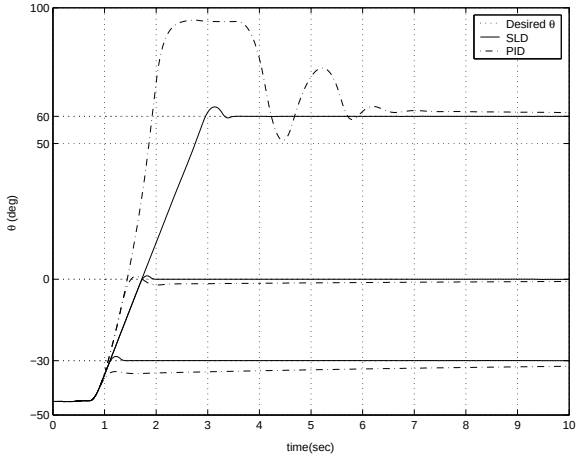

Fig. 5. Comparing the regulation performance of the feedforward-feedback controller (SLD) with a PID controller

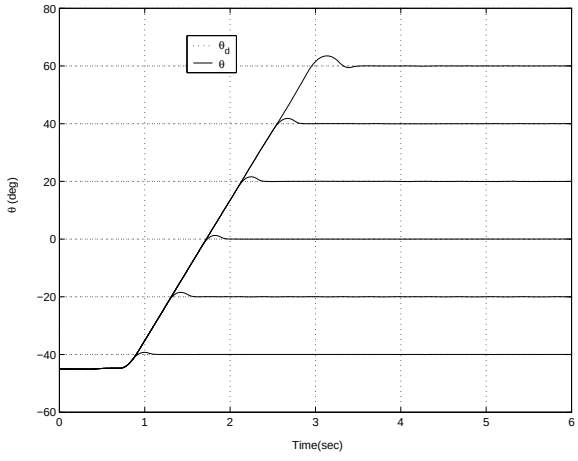

Fig. 6. The regulation performance of the feedforward-feedback controller (SLD) for desired positions $\theta_d = -40^o$ up to $\theta_d = 60^o$

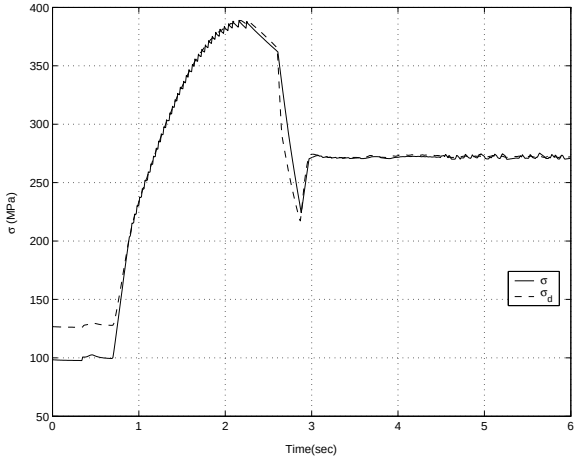

Fig. 7. The tracking performance of the feedback part of the controller following the desired stress of the wire $\theta_d = 45^o$

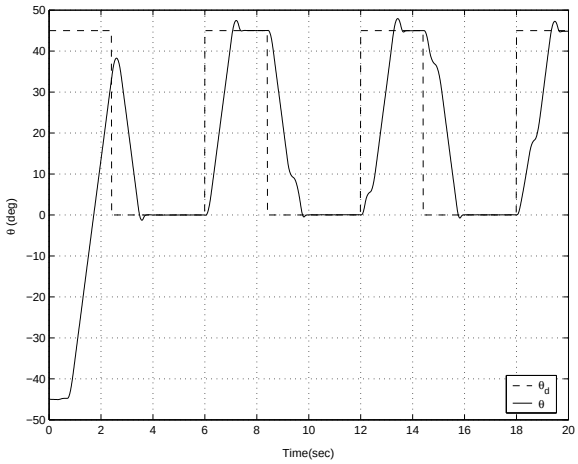

Fig. 8. The tracking performance of the feedforward-feedback controller (SLD) following a changing step input

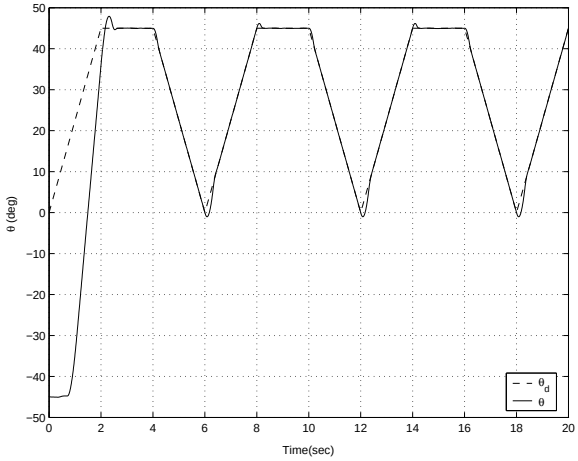

Fig. 9. The tracking performance of the feedforward-feedback controller (SLD) following a repeating step input changing between 0^o and 45^o

stress is shown in the Fig. 7. The tracking performance is good and as the result arm reaches the desired angular position.

Figures 8, 9, and 10 show the tracking performance of the controller for repeating step and ramp inputs respectively. The arm closely follows the desired angular position; however because of the speed limitation of the SMA wire, the tracking performance is better when arm follows desired position signals with smaller motion spans. Figure 11 and 12 show the tracking performance of the controller for sinusoidal inputs with two different frequencies. Although the motion span is the same for the two sinusoidal desired inputs, it can be seen that the tracking performance is better for slow varying inputs due to inherent speed limitation of the SMA wire.

Figure 13 shows the effect of the sliding surface parameter λ on the regulation performance of the controller. The sliding mode control transforms the dynamic of the system into a 1st order system $s = (\frac{d}{dt} + \lambda)\widetilde{\theta}$. Therefore increasing λ is similar to adding more damping to the system hence the overshoot decreases and the system's response gets slower. Figure 14 shows the effect of discontinuity gain K on the regulation performance of the controller. Increasing this gain is equivalent to putting more energy to the system and therefore the system responds faster and with higher overshoot; decreasing the gain has the opposite effect. Thus the performance of the controller can be augmented by adjusting the gain K and weighting factor λ of the sliding mode controller.

Figures 15 and 16 depict the robustness of the controller. The effective moment of inertia and the damping coefficient are two of the parameters that are used both in the dynamic model and the sliding mode control law (equations 1 and 14). To model uncertainties different values are used for these parameters in the sliding mode controller and in the model. From equation 14, it can be seen that if the moment of inertia used by controller $\widetilde{I}_e$ is larger than the actual moment of inertia, system's response is more damped. On the other hand if the damping coefficient used by the sliding mode controller $\widetilde{c}$ is larger than the actual c, the system responds similar to a less damped system and therefore with larger overshoot. Increasing damping coefficient results in calculating a larger desired stress, the feedback controller applies larger inputs to the wire and therefore there exists larger overshoot and faster response. In the same way, choosing a larger moment of inertia reduces the calculated desired stress and therefore the controller applies smaller voltage to the wire and hence the system responds slower and with smaller overshoot.

V. Conclusion

A sliding mode controller is designed for a rotary SMA-actuated manipulator and has been tested through simulations. This control law solves one of the challenges for control of this system (i.e. dependency of the transformation temperatures on the wire stress). The controller regulates the wire's input voltage based on the desired stress calculated by the sliding mode controller. An Extended Kalman Filter is used for estimating the SMA wire's stress. Satisfactory control results have been shown in terms of the reaching desired angular position and tracking desired trajectories. Since the model

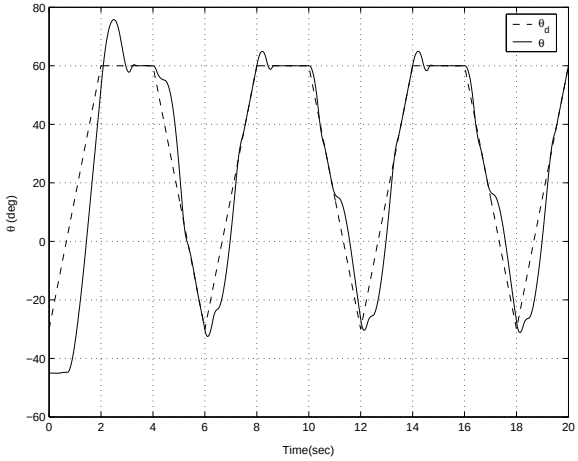

Fig. 10. The tracking performance of the feedforward-feedback controller (SLD) following a repeating step input changing between -45^o and 60^o

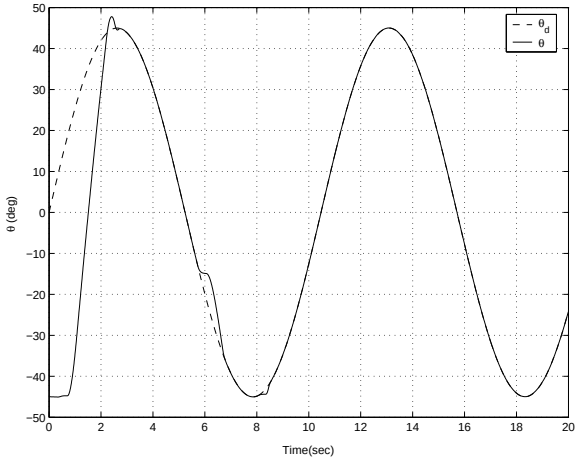

Fig. 11. The tracking performance of the feedforward-feedback controller (SLD) following a sinusoidal input with frequency $\omega = 0.6$rad/sec

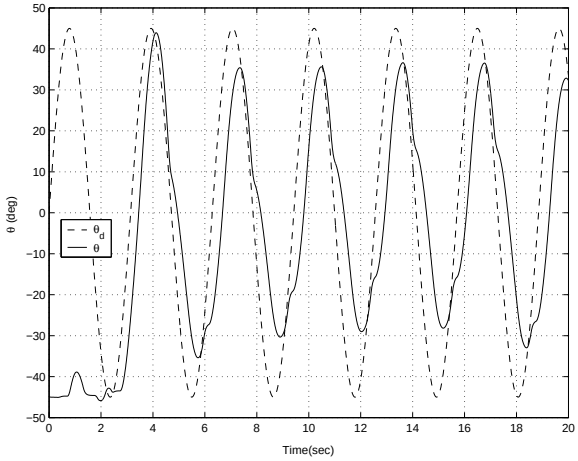

Fig. 12. The tracking performance of the feedforward-feedback controller (SLD) following a sinusoidal input with frequency $\omega = 2.0$rad/sec

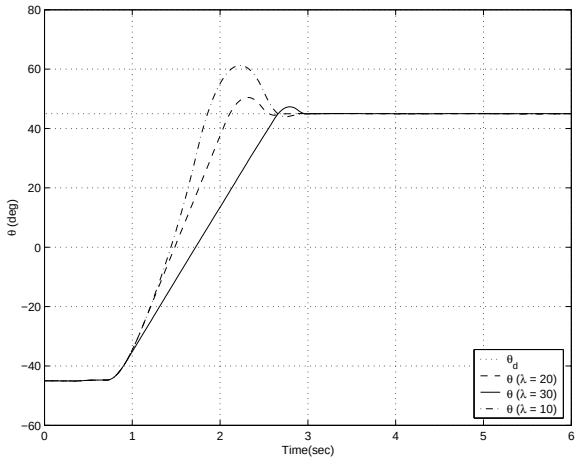

Fig. 13. Effect of the sliding surface parameter λ of the regulation performance on the controller, $K = 1$

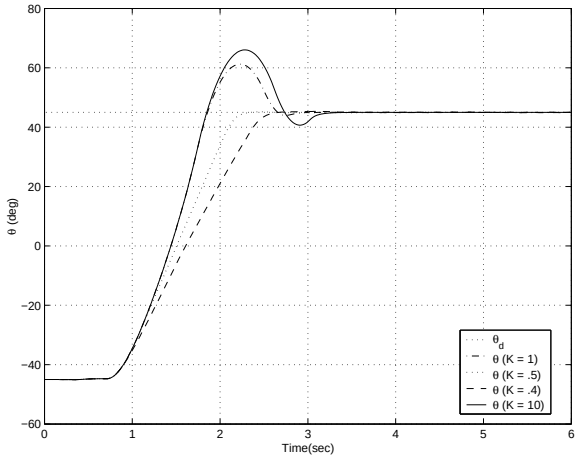

Fig. 14. Effect of the discontinuity parameter across the sliding surface K on the regulation performance of the controller, $\lambda = 30$

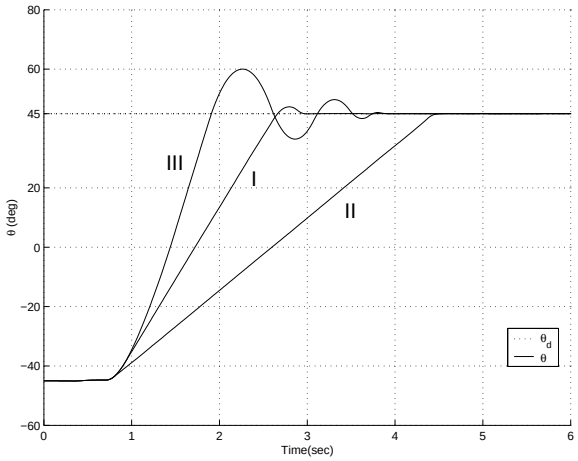

Fig. 15. Effect of the parameter (moment od inertia) uncertainty on the stabilization performance of the controller, I: $\widetilde{I_e} = I_e$, II: $\widetilde{I_e} = 2I_e$, III: $\widetilde{I_e} = 0.5I_e$, $\lambda = 30$, $K = 1$, and $\widetilde{c} = c$

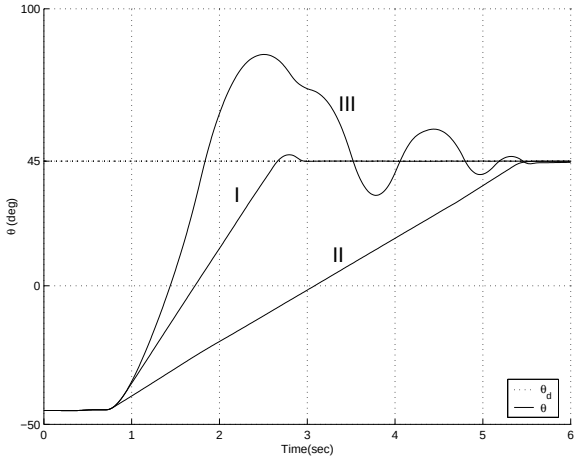

Fig. 16. Effect of the parameter (damping coefficient) uncertainty on the stabilization performance of the controller, I: $\widetilde{c} = c$, II: $\widetilde{c} = 0.5c$, III: $\widetilde{c} = 1.2c$, $\lambda = 30$, $K = 1$, and $\widetilde{I_e} = I$

had been previously verified against experimental data and the controller is designed based on this model, it is expected that the controller works well with the SMA actuated arm. It is also shown that the control performance is robust in the presence of model uncertainties.

REFERENCES

[1] S. Arai, K. Aramaki and Y. Yanagisawa. Continuous system modeling of shape memory alloy (SMA) for control analysis. *Proceedings of the 5th IEEE International Symposium on Micro Machine and Human Science*, pages 97–99, 1994.

[2] B. Carpenter, R. J. Head and R. Gehling. Shape memory-actuated gimbal. *Proceedings of SPIE - The International Society of Optical Engineering, San Diego, CA*, 2447:91–101, 1995.

[3] R. B. Gorbet and D. W. L. Wang. General stability criteria for a shape memory position control systems. *Proceedings of IEEE International Conference on Robotics and Automation*, 3:2313–2319, 1995.

[4] K. Ikuta. Micro/miniature shape memory alloy actuator. *IEEE Robotics and Automation Society, Los Alamitos, CA. IEEE Computer Society Press*, 3:2156–2161, 1990.

[5] D. Reynaerts and H. Van Brussel. Development of a SMA high performance robotic actuator. *Fifth International Conference on Advanced Robotics, New York*, 2:19–27, 1991.

[6] M. W. M. van der Wijst, P. J. G. Schreurs, and F. E. Veldpaus. Application of computed phase transformation power to control shape memory alloy actuators. *Smart Materials and Structures*, 6(2):190–198, 1997.

[7] M. A. Gharaybeh and G. C. Burdea. Investigation of a shape memory alloy actuator force-feedback masters. *Advanced Robotics*, 9(3):317–329, 1995.

[8] M. Hashimoto, M. Takeda, H. Sagawa, and I. Chiba. Application of shape memory alloy to robotic actuators. *Journal of robotic systems*, 2(1):3–25, 1985.

[9] D. Honma, Y. Miwa, and N. Iguchi. Micro robots and micro mechanisms using shape memory alloy. *The third Toyota Conference, Integrated Micro Motion Systems, Micro-machining, Control and Applications, Nissan, Aichi, Japan*, 1984.

[10] K. Kuribayashi. A new actuator of a joint mechanism using NiTi alloy wire. *The International Journal of Robotics Research*, 4(4):103–108, 1986.

[11] S. Arai, K. Aramaki and Y. Yanagisawa. Feedback linearization of SMA(Shape Memory Alloy). *Proceedings of the 34th SICE Annual Conference*, pages 519–522, 1995.

[12] S. Choi and C. C. Cheong. Vibration control of flexible beam using shape memory alloy actuators. *Journal of Guidance Control, and Dynamics*, 19(5):1178–1180, 1996.

[13] C. A. Dickinson and J. T. Wen. Feedback control using shape memory alloy actuators. *Journal of Intelligent Material Systems and Structures, Technomic Publ Co Inc, Lancaster, PA, USA*, 9(4):242–250, 1998.

[14] M. H. Elahinia and H. Ashrafiuon. Nonlinear control of a shape memory

alloy actuated manipulator. *ASME Journal of Vibration and Acoustics*, 124:566–575, October 2002.

[15] D. Grant and V. Hayward. Design of shape memory alloy actuator with high strain and variable structure control. *Proceedings of the IEEE International Conference on Robotics and Automation*, pages 2305–2310, 1995.

[16] D. Grant and V. Hayward. Vibration isolation with high strain shape memory alloy actuators: case of the impulse disturbance. *In Proceedings of International Mechanical Engineering Congress and Exposition*, 229, 1998.

[17] D. Grant and V. Hayward. Variable structure control of shape memory alloy actuators. *IEEE Systems and Control Magazine*, 17(3):80–88, 1997.

[18] D. Grant and V. Hayward. Constrained force control of shape memory alloy actuators. *Proceedings of the IEEE International Conference on Robotics and Automation*, pages 1314–1320, 2000.

[19] P. Kumagai, A. Hozian and M Kirkland. Neuro-fuzzy model based feedback controller for Shape Memory Alloy actuators. *Proceedings of SPIE - The International Society for Optical Engineering, Society of Photo-Optical Instrumentation Engineers, Bellingham, WA, USA*, 3984:291–299, 2000.

[20] T. Nakazato, Y. Kato and T. Masuda. Control of push-pull-type shape memory alloy actuators by fuzzy reasoning. *Transactions of Japan Society of Mechanical Engineers, Part C*, 59(568):226–232, 1993.

[21] G. Song, V. Chaudhry, and C. Batur. Precision tracking control of shape memory alloy actuators using neural networks and a sliding-mode based robust controller. *Journal of smart materials and structures*, 12:223–231, 2003.

[22] G. Webb, L. Wilson, D. Lagoudas, and O. Rediniotis. Adaptive control of shape memory alloy actuators for underwater biomimetic applications. *AIAA JOURNAL*, 38(2):223–231, February 2000.

[23] C. Lee and C. Mavroidis. Analytical dynamic model and experimental robust and optimal control of shape-memory-alloy bundle actuators. *Proceedings of the 2002 Symposium on Advances in Robot Dynamics and Control, ASME International Mechanical Engineering Congress and Exposition, November 17-22, 2002, New Orleans, LA, USA.*, 38(2):223–231, November 2002.

[24] C. Liang and C. A. Rogers. One-dimensional thermomechanical constitutive relations for shape memory materials. *Journal of Intelligent Material Systems and Structures*, 1(2):207–234, 1990.

[25] L. C. Brinson. One-dimensional constitutive behavior of shape memory alloys: thermomechanical derivation with non-constant material functions and redefined martensite internal variable. *Journal of intelligent material systems and structures*, 4:229–242, April 1993.

[26] Ali R. Shahin, Peter H. Meckl, James D. Jones, and Mark A. Thrasher. Enhanced cooling of shape memory alloy wires using semiconductor heat pump modules. *Journal of Intelligent Material Systems and Structures*, 5(1):95–104, 1994.

[27] M. H. Elahinia, H. Ashrafiuon, A. Ahmadian, and W. T. Baumann. Design of extended kalman filter for a shape memory alloy manipulator. *Proceedings of the ASME Design Engineering Technical Conferences, September 2-6, 2003, Chicago, Illinois*, September 2003.

[28] M. H. Elahinia, H. Ashrafiuon, A. Ahmadian, and Inman D. J. Application of the extended kalman filter to control of a shape memory alloy arm. *Proceedings of the ASME Design Engineering Technical Conferences, September 2-6, 2003, Chicago, Illinois*, September 2003.

[29] Y. Tanaka. A thermomechanical sketch of shape memory effect: One-dimensional tensile behavior. *Res Mechanica, the International Journal of Structural Machines and Materials Science*, 18(1):251–263, 1986.

[30] Jean-JAcques E. Slotine and Weiping Li. *Applied nonlinear control*. Printice-Hall International Inc., Upper saddle, NJ, 1st edition, 1990.

[31] Khalil Hassan K. *Nonlinear systems*. Simon & Shuster, Upper Saddle River, NJ 07458, 2nd edition, 1996.